ACS SENSORS

ACS Editors' Choice

Article

pubs.acs.org/acssensors

Reaction-Based Probes for Imaging Mobile Zinc in Live Cells and Tissues

Melissa L. Zastrow,[†,§] Robert J. Radford,[†,§] Wen Chyan,[†] Charles T. Anderson,[‡] Daniel Y. Zhang,[†] Andrei Loas,[†] Thanos Tzounopoulos,[‡] and Stephen J. Lippard*[,†]

[†]Department of Chemistry, Massachusetts Institute of Technology, Cambridge, Massachusetts 02139, United States

[‡]Departments of Otolaryngology and Neurobiology, University of Pittsburgh, Pittsburgh, Pennsylvania 15261, United States

Supporting Information

ABSTRACT: Chelatable, or mobile, forms of zinc play critical signaling roles in numerous biological processes. Elucidating the action of mobile Zn(II) in complex biological environments requires sensitive tools for visualizing, tracking, and manipulating Zn(II) ions. A large toolbox of synthetic photoinduced electron transfer (PET)-based fluorescent Zn(II) sensors are available, but the applicability of many of these probes is limited by poor zinc sensitivity and low dynamic ranges owing to proton interference. We present here a general approach for acetylating PET-based probes containing a variety of fluorophores and zinc-binding units. The new sensors provide substantially improved zinc sensitivity and allow for incubation of live cells and tissue slices with nM probe concentrations, a significant improvement compared to the μM concentrations that are typically required for a measurable fluorescence signal. Acetylation effectively reduces or completely quenches background fluorescence in the metal-free sensor. Binding of Zn(II) selectively and quickly mediates hydrolytic cleavage of the acetyl groups, providing a large fluorescence response. An acetylated blue coumarin-based sensor was used to carry out detailed analyses of metal binding and metal-promoted acetyl hydrolysis. Acetylated benzoresorufin-based red-emitting probes with different zinc-binding sites are effective for sensing Zn(II) ions in live cells when applied at low concentrations (~50−100 nM). We used green diacetylated Zinpyr1 (DA-ZP1) to image endogenous mobile Zn(II) in the molecular layer of mouse dorsal cochlear nucleus (DCN), confirming that acetylation is a suitable approach for preparing sensors that are highly specific and sensitive to mobile zinc in biological systems.

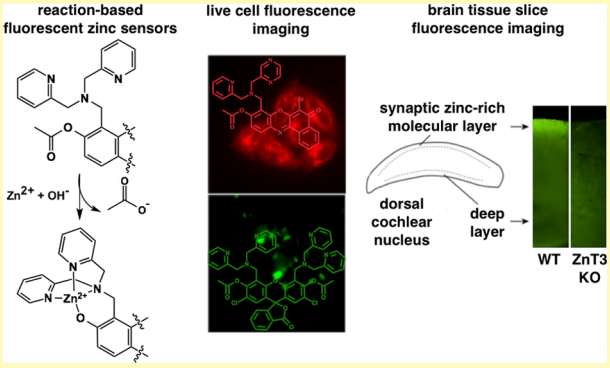

KEYWORDS: *zinc sensors, metalloneurochemistry, fluorescence, auditory synapses, ZnT3*

Zinc is an essential nutrient found in all tissues in the body. The vast majority of zinc ions are tightly bound to protein scaffolds and play key catalytic or structural roles.[1] A smaller subset of chelatable, weakly bound, or mobile zinc ions are present in high concentrations in several tissues, including the brain, pancreas, and prostate.[2−4] In particular, mobile zinc is concentrated in specific regions of the brain, including the hippocampus, amygdala, cortex, and dorsal cochlear nucleus (DCN), where it serves as a neurotransmitter/modulator.[3,5−7] In the brain, mobile Zn(II) is loaded into presynaptic vesicles of glutamatergic neurons by the zinc transporter protein ZnT3.[8] Synaptic zinc is released in response to presynaptic action potentials and modulates several ion channels and receptors, including synaptic and extrasynaptic *N*-methyl-D-aspartate receptors (NMDARs).[5,9,10]

Understanding the numerous, complex roles of mobile zinc in physiology and pathology requires adequate and sensitive tools for its detection. Currently, there is a vast collection of zinc sensors for visualizing mobile zinc in biology.[11] Among them, the largest class comprises fluorescent probes,[12] many of which rely on zinc binding to alleviate photoinduced electron transfer (PET) quenching between the chelating unit and the fluorophore, leading to fluorescence enhancement. A general drawback with these optical probes is that proton-induced background fluorescence reduces the dynamic range in a pH-dependent manner.

Previously, we showed that diacetylation (DA) of Zinpyr1 (ZP1) appended to (6-amidoethyl)triphenylphosphonium (TPP)[13] or various targeting peptides[14] effectively quenches background fluorescence by disrupting the π-conjugation of fluorescein, resulting in a substantially increased zinc-induced fluorescence response by avoiding proton-induced turn-on. In the case of DA-ZP1 derivatives, the zinc ion performs two functions: (i) its Lewis acidity promotes rapid hydrolysis of the ester groups, restoring conjugation of the fluorophore, and (ii) coordination to the two dipicolylamine (DPA) zinc-binding units attenuates PET. DA-ZP1 derivatives are also insensitive to

Received: August 10, 2015
Accepted: September 23, 2015
Published: September 23, 2015

DOI: 10.1021/acssensors.5b00022
ACS Sens. 2016, 1, 32−39

intracellular esterases over a 2 h period and, upon Zn(II) removal, the zinc-induced fluorescence is attenuated due to PET in the metal-free state.[13] Complete reversibility is precluded by removal of the acetyl groups. The ample zinc-sensitive turn-on, lack of proton-induced fluorescence, and ability to be targeted to discrete intracellular locales make DA-ZP1 derivatives ideal probes for biological imaging.

Here we inquired whether acetylation could be used as a general method for improving the sensing ability of several zinc probes, including DA-ZP1 and three other sensors built on alternative fluorophore platforms (Figure 1). To address this

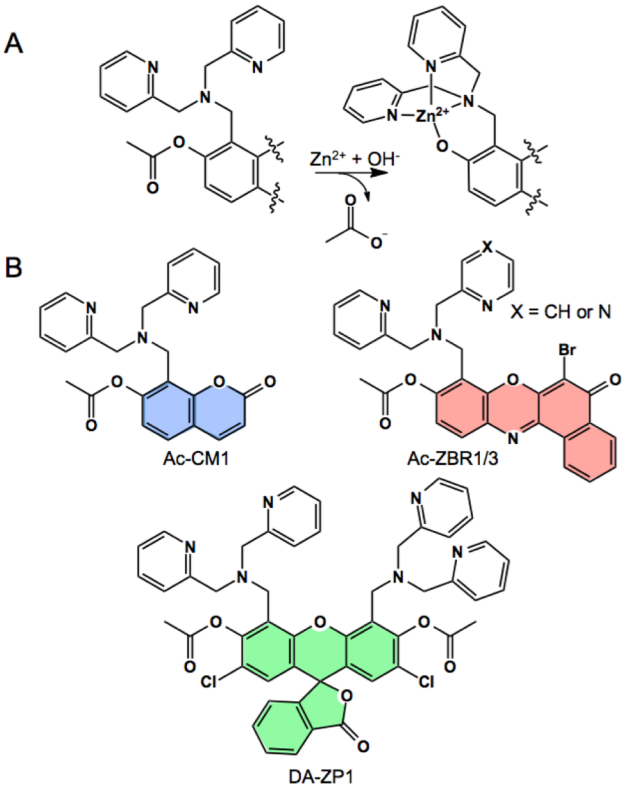

Figure 1. (A) General scheme for zinc-mediated deacetylation of fluorescent probes. (B) Chemical structures of Ac-CM1, DA-ZP1, and Ac-ZBR1/3.

question, we characterized DA-ZP1 in cuvettes, live cells, and in DCN tissue slices, as a benchmark system for acetylation. Consistent with our previous reports of DA-ZP1 conjugates,[13,14] we found that DA-ZP1 exhibits no fluorescence in the metal-free state and remains impervious to intracellular esterases for over 90 min. Additionally, DA-ZP1 accumulates preferentially in the Golgi apparatus of HeLa cells and displays high endogenous zinc-induced fluorescence signals in tissue slices. For a blue-emitting PET-based sensor, we chose a DPA functionalized 7-hydroxycoumarin (CM1),[15] which provides a single zinc-binding unit identical to those in ZP1. A single ester group, readily introduced by acetylation at the 7-position, not only effectively quenches the blue background fluorescence of the probe, but also affords a monotopic acetylated sensing platform that greatly simplifies characterization of deacetylation kinetics. Acetylated-CM1 (Ac-CM1) was employed to analyze the effects of various factors, including pH, other metals, and zinc concentration, on the rate of deacetylation. Information gained from this work should aid in the design of acetylated probes for a variety of applications.

Monotopic red-emitting sensors were also acetylated and characterized with an identical DPA zinc-binding site (ZBR3), as well as with a (2-picolyl)(pyrazin-2-yl-methyl)amine binding arm (ZBR1).[16] The ZBR probes are based on the benzophenoxazone (benzoresorufin) chromophore, which, like the 7-hydroxycoumarin and fluorescein dyes, presents an oxygen atom that can participate in the formation of an $[N_3O]$ zinc-binding motif. Our results demonstrate that acetylation can be used as an efficient general method for improving the fluorescence turn-on of Zn(II) sensors and can provide probes that are highly sensitive to mobile Zn(II) in live cells and brain tissue slices.

EXPERIMENTAL SECTION

Photophysical and Zinc-Binding Properties of Acetylated Sensors. All spectroscopic measurements were carried out in aqueous buffer (50 mM PIPES, 100 mM KCl, pH 7.0, unless otherwise indicated). Fluorescence spectra for Ac-CM1 were obtained by excitation at 355 nm and acquisition from 400 to 550 nm. For DA-ZP1, the excitation wavelength was 495 nm and emission spectra were collected from 500 to 650 nm. For Ac-ZBR1/3, excitation was at 525 nm and emission spectra were collected from 550 to 750 nm. A 0.1 s integration time was used for all acquisitions. Fluorescence data were averaged over three scans. The quantum yields were standardized to quinine sulfate in 0.1 M $H_2SO_{4(aq)}$ (λ_{ex} = 360 nm, Φ = 0.55),[17] fluorescein in 0.1 M $NaOH_{(aq)}$ (λ_{ex} = 495 nm, Φ = 0.95),[18] or resorufin in 10 mM CHES buffer, pH 9.5 (λ_{ex} = 572 nm, Φ = 0.74).[19]

Kinetics of Zinc Binding and Deacetylation. Kinetics of zinc binding to CM1 and deacetylation of Ac-CM1 were measured by monitoring the absorbance at 357 nm using either a Cary 50 UV–visible spectrophotometer (for slow kinetics), or by single-mixing stopped-flow using a Hi-Tech SF-61 DX1 double-mixing stopped-flow apparatus equipped with an absorbance detector. Buffers used were 50 mM PIPES, 100 mM KCl for pH 6.0–7.75 and 50 mM Tris, 100 mM KCl for pH 8.0–9.0. The observed rate constants (k_{obs}) obtained from all sets of experiments were calculated using Prism 5 (GraphPad Software) to fit individual traces and by averaging the results for individual fits.

Imaging Acetylated Sensors in Live HeLa Cells. The localization of acetylated sensors in HeLa was investigated by incubating the cells with Ac-CM1 (20 μM), DA-ZP1 (5 μM), Ac-ZBR1 (100 nM), or Ac-ZBR3 (125 nM), and either BODIPY TR Ceramide (1 μM), ER Tracker Green (250 nM), or MitoTracker Green (125 nM) in dye- and serum-free DMEM. After 30 min incubation at 37 °C under a humidified atmosphere with 5% CO_2, the plates were washed with 2 × 1 mL dye- and serum-free DMEM. Each plate was then bathed in 2 mL of warm dye- and serum-free DMEM and imaged by multichannel fluorescence microscopy. After acquisition of the initial set of images, the medium in the dish was replaced on stage with 2 mL of a solution of 25 μM $ZnSO_4$ and 50 μM sodium pyrithione in dye- and serum-free DMEM to increase intracellular zinc levels. After allowing the cells to reach equilibrium (~10 min), images were acquired, then the zinc-enriched medium was exchanged on the microscope stage with 2 mL of a solution of 50 μM *N*,*N*,*N*′,*N*′-tetrakis(2-pyridylmethyl)-ethylenediamine (TPEN) in dye- and serum-free DMEM, and the final set of images were acquired after 10 min. A minimum of three plates representing two passages was tested. Images acquired from at least three regions of interest for each plate were processed and quantified using ImageJ. For each measurement, the whole cell was selected as the region of interest and the integrated fluorescence from the background region was subtracted from the integrated fluorescence intensity of the cell body region. Data are presented in Figures 4, 5, S26, and S29.

Imaging Mobile Zinc Pools in Acute Slices of the Dorsal Cochlear Nucleus (DCN). All procedures using animals were approved by the Institutional Animal Care and Use Committee of the University of Pittsburgh. Male or female mice (P18–P32) were deeply anesthetized with isoflurane and decapitated. Brains were quickly removed and

DOI: 10.1021/acssensors.5b00022
ACS Sens. 2016, 1, 32–39

Table 1. Photophysical and Zinc-Binding Properties of Selected Fluorescent Zinc Sensors

	Abs: λ_{max} (nm); $\varepsilon_{max} \times 10^4$ (M^{-1} cm^{-1})		Em: λ (nm); Φ			
Sensor	Metal-free	+ Zn^{2+}	Metal-free	+ Zn^{2+}	Turn-on[a]	K_d (nM)
CM1[15]	331; 1.2	357; 1.6	451; 0.40(3)	450; 0.80(8)	3.5	0.028
Ac-CM1	286, 312	354	*b*	445; 0.84(5)	70	-
ZP1[22]	515; 7.9	507; 8.4	531; 0.38	527; 0.87	6	0.7(0.1)
DA-ZP1	*c*	505	*b*	525; 0.77(3)	291	-
ZBR1[16]	478; 1.93	530; 2.64	628	625; 0.41(3)	8.4	0.7
Ac-ZBR1	380, 455	530	627	620; 0.36(4)	42	-
ZBR3[16]	480; 1.33	535; 1.93	628	623; 0.39(4)	5	< 0.001
Ac-ZBR3	373, 454, 587	534	626	623; 0.34(2)	12.5	-

[a]The integrated emission of the Zn-coordinated divided by the Zn-free fluorophore. [b]Non-fluorescent. [c]Spectroscopically silent >400 nm.

sectioned into 210-μm-thick coronal slices containing the DCN using a vibratome (Leica). Slices were incubated in carbogenated artificial cerebrospinal fluid (ACSF) (21 mM $NaHCO_3$, 3.5 mM HEPES, 127 mM NaCl, 3 mM KCl, 2.4 mM $CaCl_2$, 1.3 mM $MgCl_2$, and 25 mM glucose; pH ~ 7.3, ~ 310 mOsm) at 35 °C for 1 h before being placed into the recording chamber. DA-ZP1 (1 μM) was added to the ACSF and allowed to equilibrate for 20 min before imaging with epifluorescent optics. DCN brain slices from WT and ZnT3 KO mice were incubated in the same chamber, with the same solution, and images were acquired at the same time. Slices were cut so that both the zinc-containing molecular layer and the zinc-free deep layer of the DCN could be visualized in the same image.[20] Images were acquired with ephus[21] and a Rolera XR CCD camera (QImaging) through a 20× immersion objective (BX, Olympus). Fluorescence of ~50 × 50 μm ROI in the deep layer was subtracted from the fluorescence of a ~50 × 50 μm ROI in the molecular layer and normalized to the fluorescence of the deep layer in the same slice.

RESULTS AND DISCUSSION

Synthesis and Photophysical Characterization. By acetylating the 7-hydroxy oxygen atom of CM1, the oxygen atoms in the 2′ and 7′ positions of the fluorescein unit in ZP1, and the oxygen atom of the benzoresorufin portion in ZBR1 or ZBR3, we produced PET-based zinc-selective sensors that are highly zinc sensitive and do not exhibit proton-induced background fluorescence. Each acetylated sensor was readily prepared by reacting the parent, either CM1,[15] ZP1,[23] ZBR1,[16] or ZBR3,[16] with acetic anhydride for several hours or overnight. Reactions were monitored by mass spectrometry or analytical HPLC to ensure completion and then purified by HPLC. The purity and identity of the four acetylated constructs were confirmed by spectroscopic and chromatographic techniques (Figures S1−S12).

The photophysical and zinc-binding properties of each sensor were examined by UV−visible absorption and fluorescence spectroscopy (Table 1 and Figure S17). First, we investigated a diacetylated (DA) version of the fluorescein-based sensor, ZP1, in the absence of a targeting vector in order to directly characterize the effects of acetylation on zinc binding, fluorescence response, and cellular localization.[13,14] DA-ZP1 is spectroscopically silent at wavelengths >400 nm and nonfluorescent. Zinc binding promotes cleavage of the acetyl groups, restoring visible absorption (λ_{max} = 505 nm) and emission (λ_{em} = 525 nm, Φ = 0.77), features consistent with those reported for zinc-bound ZP1 and DA-ZP1 conjugates.[13,14,23] The lack of background fluorescence provides a dramatic 291-fold zinc-induced turn-on, compared to a fluorescence turn-on of only ~6-fold for ZP1 upon addition of zinc.[24] When EDTA is introduced to remove zinc from the sensor, absorption and emission features identical to those reported for zinc-free ZP1 appear (λ_{abs} = 515 nm, λ_{em} = 531 nm), consistent with removal of the acetyl groups.[13,14] Next, we investigated whether acetylation of PET-based sensors with other fluorophores also quenches background fluorescence. Previously, a DPA unit was appended onto 7-hydroxycoumarin to yield a blue zinc sensor, CM1.[15] The corresponding acetylated coumarin-based probe, Ac-CM1, exhibits absorption features at 286 and 312 nm, but is nonfluorescent in the absence of zinc. Addition of Zn(II) to Ac-CM1 induces a red shift in the absorption (λ_{max} = 354 nm) and concomitant restoration of fluorescence emission (λ_{em} = 445 nm, Φ = 0.84) with a large 70-fold turn-on, an ~20-fold improvement over CM1.[15] The absorption and emission features observed are similar to those reported for Zn(II)-CM1 (Table 1). Addition of EDTA restores absorption and fluorescence features characteristic of metal-free CM1.

Next we investigated whether the acetylation strategy could be applied to red-emitting zinc sensors based on a benzoresorufin scaffold.[16] ZBR3 contains a DPA zinc-binding unit identical to those in CM1 and ZP1, but ZBR1 has a (2-picolyl)(pyrazin-2-yl-methyl)amine zinc-binding unit in which one of the pyridine rings in DPA is replaced with the more electron-withdrawing pyrazine unit. This substitution enabled us to investigate the effects of acetylation on a sensor with a different weaker affinity zinc-binding group. The K_d values for zinc-binding of sensors employing the (2-picolyl)(pyrazin-2-yl-methyl)amine binding unit(s) are generally 1 to 2 orders of magnitude lower than those observed for sensors containing one or two DPA binding arms, making them more suitable for imaging cellular environments that contain the canonical nM levels of mobile zinc.[16,25−27] Ac-ZBR1 exhibits absorption features at 380 and 455 nm and a weak fluorescence signal at 627 nm (Figure S17E). Addition of excess Zn(II) results in a rapid 42-fold increase in fluorescence with a maximum at 620 nm (Figure S17F). Subsequent addition of EDTA removes zinc and restores the absorption and emission features of ZBR1. Finally, we examined the absorption and emission characteristics of Ac-ZBR3. Three absorption features at 373, 454, and 587 nm and a modest fluorescence signal at 626 nm were observed (Figure S17G,H). Addition of zinc shifts the absorption spectrum to a single feature at 534 nm and introduces a 12.5-fold fluorescence increase at 623 nm, a better than 2-fold improvement over the parent nonacetylated ZBR3 sensor. The limited solubility of Ac-ZBR3, also observed for ZBR3,[16] may play a role in limiting its fluorescence enhancement relative to those observed for Ac-ZBR1, DA-ZP1, and Ac-CM1.

To confirm that zinc addition to each acetylated sensor led exclusively to the corresponding nonacetylated parent sensor

DOI: 10.1021/acssensors.5b00022
ACS Sens. 2016, 1, 32−39

without generating side products, we performed correlated HPLC/mass spectral analyses (Figures S13–S16). For each acetylated sensor, we prepared a sample in buffer containing either excess Zn(II) or excess EDTA. After a 5 min incubation period at room temperature to allow the deacetylation reaction to proceed to completion, the mixtures were quenched with 0.1% (v/v) TFA in water and then separated by analytical HPLC, monitoring the samples at 250 nm and the corresponding maximum absorption value for each probe (355, 520, 530, or 535 nm). Mass spectrometric analysis of each peak indicated that the EDTA-containing solutions contained only the acetylated starting material. On the other hand, in the presence of zinc, no acetylated sensor was detected and a single peak corresponding to the deacetylated sensor was observed. These results confirm that the only species obtained upon zinc addition is the parent nonacetylated sensor.

We examined the fluorescence response of Ac-CM1, DA-ZP1, and Ac-ZBR1 at different Zn(II) concentrations (<1 nM to ~25–200 nM) and found that all three sensors detect nM concentrations of mobile zinc (Figure S18). As previously reported for ZP1 and DA-ZP1-TPP, Ac-CM1 and Ac-ZBR1 have Zn(II)-selective fluorescence responses over other biologically relevant cations, including Mg(II), Ca(II), and first-row transition metal ions Mn(II), Co(II), Ni(II), and Cu(II) (Figure S19). Although these paramagnetic metal ions can bind and quench fluorescence emission, they are not readily available in free form in cells.[28] Cd(II) produces a small fluorescence response, but cadmium is not expected to be present in healthy eukaryotic cells. As discussed in the next section, by using UV–visible absorption spectroscopy, we found that some of these metal ions can, like Zn(II), promote the hydrolysis of the acetyl group, but none can match the rate of Zn(II)-promoted deacetylation (Table S2).

We examined the pH-sensitivity of zinc-promoted deacetylation for each acetylated sensor using fluorescence spectroscopy. In contrast to nonacetylated ZP1 and corresponding conjugates, DA-ZP1 does not undergo significant turn-on under acidic conditions, which greatly facilitates the imaging of mobile zinc in acidic vesicles and compartments (Figure S20). PET-based sensors like ZP1 rely on quenching originating typically from nitrogen lone pair electrons of DPA and similar zinc-binding units.[12] At low pH, one or more of the nitrogen atoms may become protonated, interfering with PET to produce increased background fluorescence. Acetylation with concomitant formation of the nonfluorescent lactone ring in DA-ZP1 introduces a stronger quenching mechanism that abolishes proton-induced fluorescence. Similarly, no significant fluorescence response was observed for Ac-CM1, Ac-ZBR1, and Ac-ZBR3 under acidic conditions.

Ac-CM1, DA-ZP1, and Ac-ZBR1/3 are readily synthesized, display strong fluorescence responses upon Zn(II) binding, are selective for Zn(II) over other transition metal cations, and display no proton-induced fluorescence. These results suggest that acetylation of PET-based probes for mobile Zn(II) may be a general method for improving the sensitivity of fluorescence for zinc imaging in biological milieu.

Kinetics of Zinc-Promoted Deacetylation. Acetylated CM1 not only extends our sensor acetylation methodology to include a blue fluorophore, but its monotopic nature, by comparison to the ditopic ZP1 probe, allows for a straightforward investigation of the kinetic properties of the zinc-promoted deacetylation reaction. Initially, we monitored the deacetylation kinetics of Ac-CM1, Ac-ZBR1, and DA-ZP1 by UV–visible absorption spectroscopy in order to examine the reaction by a means independent of the fluorescence response. Comparison of the kinetic traces for zinc-promoted deacetylation of Ac-CM1, Ac-ZBR1, and DA-ZP1 at pH 7.0 highlights the complex multistep deacetylation of DA-ZP1 as compared to simpler single exponential kinetic responses observed for monotopic Ac-CM1 and Ac-ZBR1 (Figure 2). Notably, similar

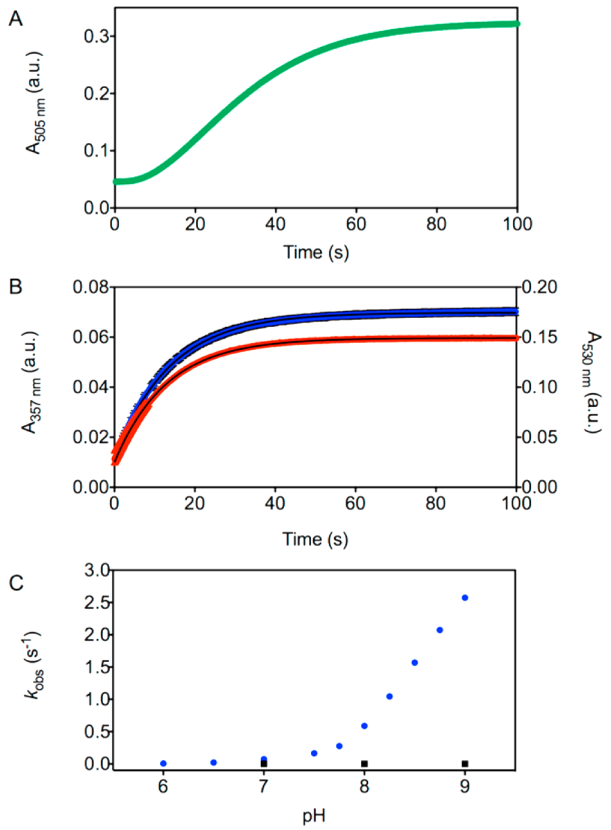

Figure 2. Zinc-induced hydrolysis of acetylated zinc sensors. Representative stopped flow kinetic trace for the deacetylation of (A) 5 μM DA-ZP1 and stopped flow kinetic traces (mean ± SD) for the deacetylation of (B) 5 μM Ac-ZBR1 (red, N = 3) and 5 μM Ac-CM1 (blue, N = 6) with excess Zn(II) (50 μM) monitored by the absorbance at 505, 530, and 357 nm, respectively (25 °C, 50 mM PIPES, 100 mM KCl, pH 7.0). (C) Plot of observed pseudo-first-order rate constants for the zinc-mediated deacetylation of 5 μM Ac-CM1 (50 μM $ZnSO_4$) as a function of pH from 6.0 to 9.0 (blue circles, $N \geq 6$ for each pH) and the spontaneous hydrolysis of 5 μM Ac-CM1 at pH 7.0, 8.0, and 9.0 (black squares, N = 3 for each pH) in aqueous buffer (50 mM PIPES, 100 mM KCl, pH 6.0–7.75; 50 mM Tris, 100 mM KCl, pH 8.0–9.0).

rates were observed for Ac-CM1 (k_{obs} = 7.26(2) × 10^{-2} s^{-1}) and Ac-ZBR1 (k_{obs} = 7.73(6) × 10^{-2} s^{-1}) at pH 7.0. We chose Ac-CM1 as a platform for more detailed kinetic studies. To characterize its deacetylation, we measured the rate of turn-on following addition of excess zinc by monitoring the increase in absorbance at 357 nm. Stopped-flow spectroscopy was employed to provide accurate measurement of the rapid hydrolysis at 25 °C. We varied the concentration of zinc relative to that of the sensor and observed no change in the deacetylation rate from 2.5- to 15-fold excess zinc (Figure S22). Next, we measured the rate of zinc binding to nonacetylated CM1. Because this binding event is very rapid at 25 °C, we performed these studies at 10 °C. Variation of the

DOI: 10.1021/acssensors.5b00022
ACS Sens. 2016, 1, 32–39

concentration of excess zinc (>10-fold) yielded pseudo-first-order rate constants that were plotted versus [Zn(II)]. From the slope of the plot we obtained the second-order rate constant, 7.98 (±0.14) × 10^5 M^{-1} s^{-1} (Figure S21). Given that both Ac-CM1 and CM1 share a similar [N_3O] binding motif, with the caveat that the oxygen atom in CM1 is in the form of a phenolate whereas that in Ac-CM1 is part of an ester group, this result suggests that the rate of zinc binding to Ac-CM1 at 25 °C will be much faster than deacetylation of Ac-CM1 (k_{obs} = 7.26(2) × 10^{-2} s^{-1}) at the same temperature and is probably not rate-limiting.

Pseudo-first-order rate constants for zinc-mediated deacetylation were measured from pH 6.0 to 9.0. The rates increased significantly with increasing pH, from 0.006 s^{-1} to 2.57 s^{-1}, which corresponds to half-lives ranging from 115 to 0.27 s, respectively (Figures 2, S23, and Table S1). Spontaneous hydrolysis occurs very slowly in the absence of zinc and was measured at pH 7.0, 8.0, and 9.0. Although an increase in the pseudo-first-order rate constant does occur with increasing pH, the rates are negligible compared to those measured in the presence of zinc. Even at pH 9.0, the measured half-life of 112 min was nearly 60-times greater than that for the slowest zinc-mediated deacetylation, which was observed at pH = 6.0 with $t_{1/2}$ = 115 s (Figures 2, S24, and Table S1).

To investigate whether the hydrolysis of acetyl groups could be promoted effectively by other transition metal ions, a 10-fold excess of the metal salt (Co(II), Cd(II), Fe(II), Mn(II), Cu(II), or Ni(II)) was added to solutions of Ac-CM1 in aqueous buffer and the observed rate constants were compared to that for Zn(II) at pH 7.0 (Figures 3, S25, and Table S2). Zn(II)

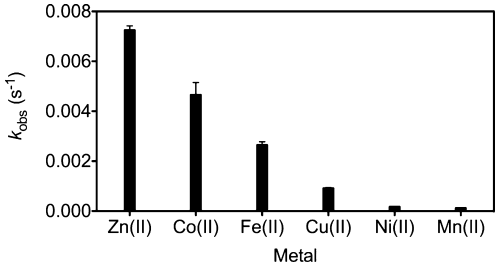

Figure 3. Observed pseudo-first-order rate constants for metal-mediated deacetylation of 5 μM Ac-CM1 (50 μM metal salt) in aqueous buffer (50 mM PIPES, 100 mM KCl, pH 7.0).

kinetically outcompetes Co(II), Fe(II), Mn(II), Cu(II), and Ni(II) for the deacetylation of Ac-CM1. Minimal hydrolytic activity was observed for Mn(II) and Ni(II), whereas more rapid deacetylation rates were recorded for Co(II), Fe(II), and Cu(II), consistent with hydrolytic activity reported for related complexes of these metal ions.[29−32] Although the rates for Co(II), Fe(II), and Cu(II) are higher than those of Mn(II) and Ni(II), they remain slower than that of Zn(II), suggesting an overall kinetic preference for this ion. Cd(II) also hydrolyzes Ac-CM1 with a slower rate than that of Zn(II), but, unlike all other metals examined, the kinetic trace did not fit a single exponential function, implying a different kinetic mechanism (see SI for further details). Collectively, these results demonstrate that sensor acetylation employing a DPA-based [N_3O] zinc-binding site not only retains the zinc selectivity afforded by the parent sensor, CM1, as evidenced by fluorescence emission, but also incorporates a kinetic preference for Zn(II)-promoted deacetylation.

Live HeLa Cell Imaging. To assess the ability of the acetylated zinc sensors to detect mobile zinc in cells, we performed live cell imaging experiments with each probe in HeLa. As with CM1, Ac-CM1 is not taken up by these cells, and therefore no initial fluorescence signal or zinc response was observed (Figure S26). DA-ZP1 effectively crosses the cell membrane, however, and, consistent with the low concentration of endogenous zinc in HeLa,[33] no significant background fluorescence was observed after a 30 min treatment with a 5 μM solution of DA-ZP1 (Figure 4). After the medium

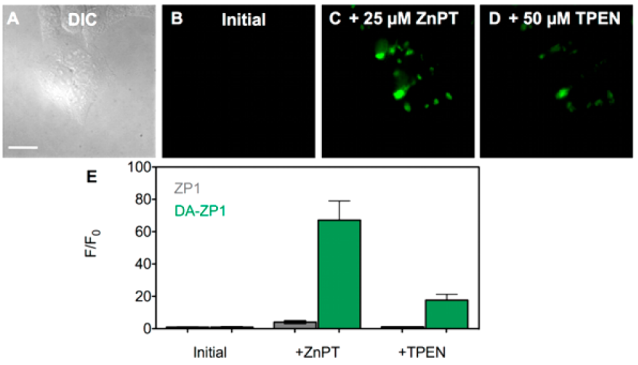

Figure 4. Fluorescence microscopy images of live HeLa cells pretreated with 5 μM DA-ZP1. (A) Differential interference contrast (DIC) image, (B) green channel fluorescence signal from DA-ZP1 initially, (C) with addition of 25 μM ZnPT, and (D) with addition of 50 μM TPEN. (E) Quantification of the change in fluorescence signal intensity of DA-ZP1 (green) compared with ZP1 (gray) (mean ± SD, N = 34). Scale bar: 25 μm.

was replaced with a solution of Zn(II) and sodium pyrithione (ZnPT) in dye- and serum-free DMEM to enrich the intracellular mobile zinc content, a large fluorescence turn-on was observed. Application of TPEN, an intracellular zinc chelator, reversed the fluorescence signal to the proton-induced background level. Quantification of the intracellular fluorescence enhancement of DA-ZP1 revealed an ∼70-fold increase, which is more than 10 times higher than that observed for nonacetylated ZP1.

We also investigated whether spontaneous hydrolysis of the acetyl groups could occur in the absence of zinc by monitoring the initial fluorescence levels for 90 min prior to adding ZnPT (Figure S27). No appreciable fluorescence turn-on was observed over this time period, and subsequent introduction of exogenous zinc led to high (>70-fold) turn-on, similar to that observed immediately following sensor incubation. We tested Ac-ZBR3 (125 nM) in a similar manner, recording the initial, ZnPT-induced, and TPEN-sensitive fluorescence signals (Figure S29). Quantification of these data yielded a zinc-induced turn-on (2.5 ± 0.7) similar to that observed for the parent sensor, ZBR3, but obtained by bathing the cells in a solution of sensor that is 40-fold more dilute than the one reported for nonacetylated ZBR3.[16] This feature afforded by sensor acetylation is attractive because it offers improved solubility and the ability to bathe the cells at lower probe concentrations. Using less sensor reduces the possibility of altering zinc homeostasis, for zinc sensors can chelate and alter the cellular levels of mobile zinc, especially when applied at high concentrations.[33,34] Few other examples of small molecule sensors that are effective at nM levels are known, including the zinc sensor ZincBY-1, which was used at 50 nM for imaging

DOI: 10.1021/acssensors.5b00022
ACS Sens. 2016, 1, 32−39

zinc in mammalian eggs.[35] Furthermore, using lower loading concentrations of cell-permeable sensors can reduce the risk of probe toxicity. Finally, we examined the intracellular response of Ac-ZBR1 in HeLa by bathing cells in a solution of 100 nM sensor. Measurement of the initial, ZnPT-induced, and TPEN-sensitive fluorescence signals revealed that, even with a sensor incubation concentration 50 times lower than that reported for ZBR1, a similar turn-on of ~6-fold occurred (Figure 5). As in

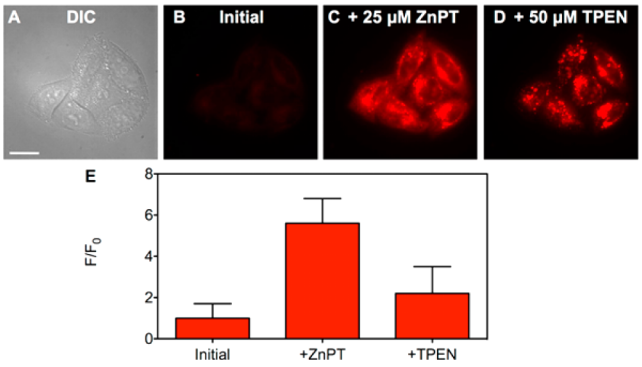

Figure 5. Fluorescence microscopy images of live HeLa cells pretreated with 100 nM Ac-ZBR1. (A) DIC image, (B) red channel fluorescence signal from Ac-ZBR1 initially, (C) with addition of 25 μM ZnPT, and (D) with addition of 50 μM TPEN. (E) Quantification of the change in fluorescence signal intensity of Ac-ZBR1 (mean ± SD, N = 165). Scale bar: 25 μm.

the case of DA-ZP1, we measured spontaneous hydrolysis of Ac-ZBR1 by recording the fluorescence levels every 15 min for 90 min prior to the addition of zinc (Figure S28). Consistent with our observations for DA-ZP1, minimal spontaneous hydrolysis occurred, confirming that deacetylation is zinc-sensitive but is impervious to intracellular esterases in HeLa cells, at least over the time scale of our experiment.

Because changes in the chemical structure of a probe can radically alter its cellular localization,[36] we examined the subcellular localization of DA-ZP1, Ac-ZBR1, and Ac-ZBR3 by coincubation with various organelle trackers. DA-ZP1 was coincubated with the Golgi tracker BODIPY TR Ceramide, because ZP1 is known to localize to the Golgi apparatus.[22,23,37] Quantitative analysis of the deconvoluted microscopy images confirmed that acetylation of ZP1 did not alter this behavior in HeLa (Figure 6, Pearson's r = 0.64 ± 0.09). Ac-ZBR1 and Ac-ZBR3 were both coincubated with ER Tracker Green. Pearson's correlation coefficients of 0.53 ± 0.07 (Figure 7, Ac-ZBR1) and 0.64 ± 0.09 (Figure S30, Ac-ZBR3) indicate moderate to strong colocalization, consistent with previous results for the corresponding nonacetylated parent sensors.[16]

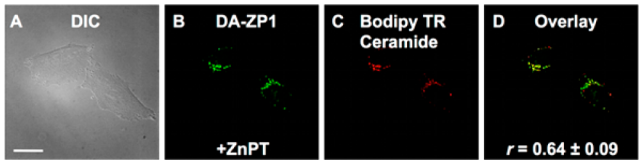

Figure 6. Deconvoluted fluorescence microscopy images of live HeLa cells pretreated with 500 nM DA-ZP1 and 1 μM BODIPY TR Ceramide. (A) DIC image, (B) fluorescence signal from DA-ZP1 after addition of 25 μM ZnPT, (C) signal from BODIPY TR Ceramide, and (D) overlay of (B) and (C). Pearson's r = 0.64 ± 0.09 (mean ± SD, N = 103). Scale bar: 25 μm.

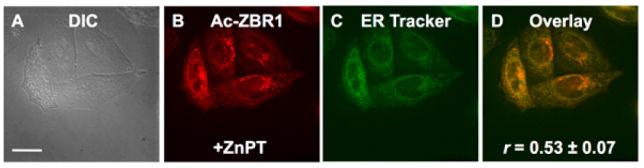

Figure 7. Deconvoluted fluorescence microscopy images of live HeLa cells pretreated with 100 nM Ac-ZBR1 and 250 nM ER Tracker Green. (A) DIC image, (B) fluorescence signal from Ac-ZBR1 after addition of 25 μM ZnPT, (C) signal from ER Tracker Green, and (D) overlay of (B) and (C). Pearson's r = 0.53 ± 0.07 (mean ± SD, N = 56). Scale bar: 25 μm.

Thus, fluorescence microscopy imaging of acetylated probes in live HeLa cells revealed their stability toward the action of intracellular esterases and a significant zinc-induced turn-on. Acetylated sensors can be applied to live cells at concentrations that are more than an order of magnitude lower than their nonacetylated counterparts, presumably due to enhanced probe solubility and cellular permeability, providing fluorescence turn-on levels at least as high or higher than that of the parent sensors.

Application of DA-ZP1 to Imaging Zinc in Brain Tissue Slices. To confirm that the acetylated sensors could detect endogenous sources of mobile zinc, we applied DA-ZP1 to acute brain slices of the mouse dorsal cochlear nucleus (DCN), a cerebellum-like structure in the auditory brainstem.[38] Unique among auditory brainstem nuclei, the molecular layer of the DCN has high levels of ZnT3-dependent, synaptic zinc.[20,39] Synaptic zinc acts as a neuromodulatory neurotransmitter in the DCN that inhibits extrasynaptic NMDARs[9] and triggers endocannabinoid release via activation of GPR39, a metabotropic zinc receptor.[40] Because high levels of synaptic zinc are restricted to the molecular layer of the DCN,[20,39] the DCN is well suited for studying the efficacy and specificity of our new cell-permeable zinc sensor DA-ZP1. We prepared acute DCN slices (Figure 8A) and incubated them for 20 min in ACSF containing 1 μM DA-ZP1. Fluorescence microscopy imaging revealed increased fluorescence in the synaptic zinc-rich molecular layer, but not in the zinc-free deep layer (Figure 8B). Importantly, in brain slices prepared from ZnT3 KO mice that lack synaptic zinc, the molecular layer did not show

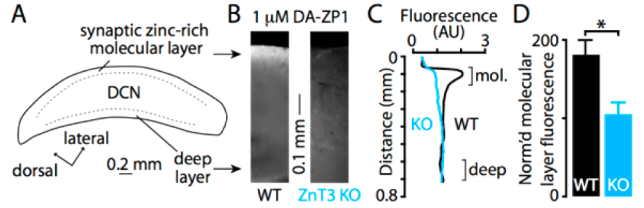

Figure 8. (A) Drawing of a DCN slice showing location of synaptic zinc-rich molecular layer and the synaptic zinc-lacking deep layer. (B) Fluorescence images of DCN slices incubated with 1 μM DA-ZP1 in ACSF for 20 min. The synaptic zinc-rich molecular layer of the DCN shows increased fluorescence compared to the zinc-free deep layer in WT mice, but the fluorescence was homogeneous in both layers in ZnT3 KO mice. (C) Quantification of the radial fluorescence profile in B shows the molecular layer has increased fluorescence in WT but not in ZnT3 KO, indicating that DA-ZP1 detects synaptic zinc. (D) Group data showing that WT mice have significantly higher molecular layer fluorescence than ZnT3 KO mice (WT = 181.1 ± 18.7%, ZnT3 KO = 103.9 ± 16.1%, p = 0.019, t test, N = 4, fluorescence values are normalized to fluorescence levels in the deep layer).

DOI: 10.1021/acssensors.5b00022
ACS Sens. 2016, 1, 32−39

fluorescence greater than other regions of the slice (Figure 8C). Group data revealed that the WT DCN had significantly stronger DA-ZP1 mediated fluorescent signals in the synaptic zinc-rich molecular layer than the ZnT3 KO DCN (Figure 8D). Sensor acetylation allows us to incubate slices at 1 μM concentrations, an order-of-magnitude less than that previously reported for imaging brain tissue slices, and observe strong fluorescence signals.[24] These results demonstrate that DA-ZP1 is well suited for detecting chelatable zinc in acute brain slices.

CONCLUSIONS

Acetylation of fluorescent zinc sensors is a robust method for improving the turn-on and allowing for incubation of live cells and tissue slices with much lower sensor concentrations, therefore avoiding perturbation of metal homeostasis. Blue coumarin-, green fluorescein-, and red benzoresorufin-based zinc sensors can be readily acetylated in a single-step synthesis and purified by HPLC. These sensors display pH profiles advantageous for biological imaging applications, are zinc-selective, and are partially reversible owing to PET-based fluorescence quenching from the zinc-binding group. Kinetic analysis of zinc-mediated hydrolysis of Ac-CM1 shows that zinc kinetically outcompetes other late first-row transition metal ions. The pH sensitivity profile indicates that alterations to the zinc-binding site to decrease the estimated pK_a for hydrolysis can tune the rate of deacetylation. For example, one may desire a sensor that will be hydrolyzed at a rate commensurate with the pH of the organelle in which it accumulates (e.g., the mitochondrial matrix at pH 8 versus secretory vesicles at pH ~ 5.5).[41] Furthermore, addition of the acetyl group does not alter sensor localization in live HeLa cells, and acetylated sensors can be employed at concentrations approximately 10-fold lower than nonacetylated analogs. Finally, using DA-ZP1, we obtained the first images of vesicular zinc in acute brain slices of the DCN.

ASSOCIATED CONTENT

Supporting Information

The Supporting Information is available free of charge on the ACS Publications website at DOI: 10.1021/acssensors.5b00022.

Additional experimental methods, NMR spectra, analytical HPLC spectra, mass spectra, zinc sensitivity graphs, metal selectivity graphs, pH sensitivity graphs, kinetic data, and cell imaging experiments (PDF)

AUTHOR INFORMATION

Corresponding Author

*E-mail: lippard@mit.edu.

Author Contributions

[§]Melissa L. Zastrow and Robert J. Radford contributed equally.

Notes

The authors declare no competing financial interest.

ACKNOWLEDGMENTS

This work was supported by grants from the National Institutes of Health GM065519 (to S.J.L.) and R01-DC007905 (to T.T.). We also acknowledge NIH fellowship support to M.L.Z. (F32-EB019243) and C.T.A. (T32-DC011499 and F32-DC013734).

REFERENCES

(1) Bertini, I.; Gray, H. B.; Stiefel, E. I.; Valentine, J. S. *Biological Inorganic Chemistry: Structure and Reactivity*; University Science Books: Sausalito, CA, 2007.

(2) Costello, L. C.; Fenselau, C. C.; Franklin, R. B. Evidence for Operation of the Direct Zinc Ligand Exchange Mechanism for Trafficking, Transport, and Reactivity of Zinc in Mammalian Cells. *J. Inorg. Biochem.* **2011**, *105*, 589−599.

(3) Sensi, S. L.; Paoletti, P.; Koh, J.-Y.; Aizenman, E.; Bush, A. I.; Hershfinkel, M. The Neurophysiology and Pathology of Brain Zinc. *J. Neurosci.* **2011**, *31*, 16076−16085.

(4) Kelleher, S. L.; McCormick, N. H.; Velasquez, V.; Lopez, V. Zinc in Specialized Secretory Tissues: Roles in the Pancreas, Prostate, and Mammary Gland. *Adv. Nutr.* **2011**, *2*, 101−111.

(5) Paoletti, P.; Vergnano, A. M.; Barbour, B.; Casado, M. Zinc at Glutamatergic Synapses. *Neuroscience* **2009**, *158*, 126−136.

(6) Sensi, S. L.; Paoletti, P.; Bush, A. I.; Sekler, I. Zinc in the Physiology and Pathology of the CNS. *Nat. Rev. Neurosci.* **2009**, *10*, 780−791.

(7) Tóth, K. Zinc in Neurotransmission. *Annu. Rev. Nutr.* **2011**, *31*, 139−153.

(8) Palmiter, R. D.; Cole, T. B.; Quaife, C. J.; Findley, S. D. ZnT-3, a Putative Transporter of Zinc into Synaptic Vesicles. *Proc. Natl. Acad. Sci. U. S. A.* **1996**, *93*, 14934−14939.

(9) Anderson, C. T.; Radford, R. J.; Zastrow, M. L.; Zhang, D. Y.; Apfel, U.-P.; Lippard, S. J.; Tzounopoulos, T. Modulation of Extrasynaptic NMDA Receptors by Synaptic and Tonic Zinc. *Proc. Natl. Acad. Sci. U. S. A.* **2015**, *112*, E2705−E2714.

(10) Pan, E.; Zhang, X. A.; Huang, Z.; Krezel, A.; Zhao, M.; Tinberg, C. E.; Lippard, S. J.; McNamara, J. O. Vesicular Zinc Promotes Presynaptic and Inhibits Postsynaptic Long-Term Potentiation of Mossy Fiber-CA3 Synapse. *Neuron* **2011**, *71*, 1116−1126.

(11) Carter, K. P.; Young, A. M.; Palmer, A. E. Fluorescent Sensors for Measuring Metal Ions in Living Systems. *Chem. Rev.* **2014**, *114*, 4564−4601.

(12) Wong, B. A.; Friedle, S.; Lippard, S. J. Solution and Fluorescence Properties of Symmetric Dipicolylamine-Containing Dichlorofluorescein-Based Zn^{2+} Sensors. *J. Am. Chem. Soc.* **2009**, *131*, 7142−7152.

(13) Chyan, W.; Zhang, D. Y.; Lippard, S. J.; Radford, R. J. Reaction-Based Fluorescent Sensor for Investigating Mobile Zn^{2+} in Mitochondria of Healthy versus Cancerous Prostate Cells. *Proc. Natl. Acad. Sci. U. S. A.* **2014**, *111*, 143−148.

(14) Radford, R. J.; Chyan, W.; Lippard, S. J. Peptide Targeting of Fluorescein-Based Sensors to Discrete Intracellular Locales. *Chem. Sci.* **2014**, *5*, 4512−4516.

(15) Mizukami, S.; Okada, S.; Kimura, S.; Kikuchi, K. Design and Synthesis of Coumarin-Based Zn^{2+} Probes for Ratiometric Fluorescence Imaging. *Inorg. Chem.* **2009**, *48*, 7630−7638.

(16) Lin, W.; Buccella, D.; Lippard, S. J. Visualization of Peroxynitrite-Induced Changes of Labile Zn^{2+} in the Endoplasmic Reticulum with Benzoresorufin-Based Fluorescent Probes. *J. Am. Chem. Soc.* **2013**, *135*, 13512−13520.

(17) Eastman, J. W. Quantitative Spectrofluorimetry-the Fluorescence Quantum Yield of Quinine Sulfate. *Photochem. Photobiol.* **1967**, *6*, 55−72.

(18) Lakowicz, J. R. *Principles of Fluorescence Spectroscopy*, 2nd ed.; Kluwer Academic/Plenum: New York, 1999; p 698.

(19) Bueno, C.; Villegas, M. L.; Bertolotti, S. G.; Previtali, C. M.; Neumann, M. G.; Encinas, M. V. The Excited-State Interaction of Resazurin and Resorufin with Amines in Aqueous Solutions. Photophysics and Photochemical Reactions. *Photochem. Photobiol.* **2002**, *76*, 385−390.

(20) Rubio, M. E.; Juiz, J. M. Chemical Anatomy of Excitatory Endings in the Dorsal Cochlear Nucleus of the Rat: Differential Synaptic Distribution of Aspartate Aminotransferase, Glutamate, and Vesicular Zinc. *J. Comp. Neurol.* **1998**, *399*, 341−358.

(21) Suter, B. A.; O'Connor, T.; Iyer, V.; Petreanu, L. T.; Hooks, B. M.; Kiritani, T.; Svoboda, K.; Shepherd, G. M. G. Ephus: Multipurpose

DOI: 10.1021/acssensors.5b00022
ACS Sens. 2016, 1, 32−39

Data Acquisition Software for Neuroscience Experiments. *Front. Neural Circuits* **2010**, *4*, 100.
(22) Nolan, E. M.; Lippard, S. J. Small-Molecule Fluorescent Sensors for Investigating Zinc Metalloneurochemistry. *Acc. Chem. Res.* **2009**, *42*, 193−203.
(23) Burdette, S. C.; Walkup, G. K.; Spingler, B.; Tsien, R. Y.; Lippard, S. J. Fluorescent Sensors for Zn^{2+} Based on a Fluorescein Platform: Synthesis, Properties and Intracellular Distribution. *J. Am. Chem. Soc.* **2001**, *123*, 7831−7841.
(24) Huang, Z.; Lippard, S. J. Illuminating Mobile Zinc with Fluorescence from Cuvettes to Live Cells and Tissues. *Methods Enzymol.* **2012**, *505*, 445−468.
(25) Buccella, D.; Horowitz, J. A.; Lippard, S. J. Understanding Zinc Quantification with Existing and Advanced Ditopic Fluorescent Zinpyr Sensors. *J. Am. Chem. Soc.* **2011**, *133*, 4101−4114.
(26) Rivera-Fuentes, P.; Wrobel, A. T.; Zastrow, M. L.; Khan, M.; Georgiou, J.; Luyben, T. T.; Roder, J. C.; Okamoto, K.; Lippard, S. J. A Far-Red Emitting Probe for Unambiguous Detection of Mobile Zinc in Acidic Vesicles and Deep Tissue. *Chem. Sci.* **2015**, *6*, 1944−1948.
(27) Zhang, X.-a.; Hayes, D.; Smith, S. J.; Friedle, S.; Lippard, S. J. New Strategy for Quantifying Biological Zinc by a Modified Zinpyr Fluorescence Sensor. *J. Am. Chem. Soc.* **2008**, *130*, 15788−15789.
(28) Finney, L. A.; O'Halloran, T. V. Transition Metal Speciation in the Cell: Insights from the Chemistry of Metal Ion Receptors. *Science* **2003**, *300*, 931−936.
(29) Au-Yeung, H. Y.; New, E. J.; Chang, C. J. A Selective Reaction-Based Fluorescent Probe for Detecting Cobalt in Living Cells. *Chem. Commun.* **2012**, *48*, 5268−5270.
(30) Kierat, R. M.; Krämer, R. A Fluorogenic and Chromogenic Probe that Detects the Esterase Activity of Trace Copper(II). *Bioorg. Med. Chem. Lett.* **2005**, *15*, 4824−4827.
(31) Mancin, F.; Scrimin, P.; Tecilla, P. Progress in Artificial Metallonucleases. *Chem. Commun.* **2012**, *48*, 5545.
(32) Suh, J. 6.27 - Artificial Metalloproteases and Metallonucleases. In *Comprehensive Inorganic Chemistry II*, 2nd ed.; Poeppelmeier, J. R., Ed.; Elsevier: Amsterdam, 2013; pp 779−803.
(33) Qin, Y.; Miranda, J. G.; Stoddard, C. I.; Dean, K. M.; Galati, D. F.; Palmer, A. E. Direct Comparison of a Genetically Encoded Sensor and Small Molecule Indicator: Implications for Quantification of Cytosolic Zn^{2+}. *ACS Chem. Biol.* **2013**, *8*, 2366−2371.
(34) Dineley, K. E.; Malaiyandi, L. M.; Reynolds, I. J. A Reevaluation of Neuronal Zinc Measurements: Artifacts Associated with High Intracellular Dye Concentration. *Mol. Pharmacol.* **2002**, *62*, 618−627.
(35) Que, E. L.; Bleher, R.; Duncan, F. E.; Kong, B. Y.; Gleber, S. C.; Vogt, S.; Chen, S.; Garwin, S. A.; Bayer, A. R.; Dravid, V. P.; Woodruff, T. K.; O'Halloran, T. V. Quantitative Mapping of Zinc Fluxes in the Mammalian Egg Reveals the Origin of Fertilization-Induced Zinc Sparks. *Nat. Chem.* **2014**, *7*, 130−139.
(36) Loas, A.; Radford, R. J.; Lippard, S. J. Addition of a Second Binding Site Increases the Dynamic Range but Alters the Cellular Localization of a Red Fluorescent Probe for Mobile Zinc. *Inorg. Chem.* **2014**, *53*, 6491−6493.
(37) Walkup, G. K.; Burdette, S. C.; Lippard, S. J.; Tsien, R. Y. A New Cell-Permeable Fluorescent Probe for Zn^{2+}. *J. Am. Chem. Soc.* **2000**, *122*, 5644−5645.
(38) Oertel, D.; Young, E. D. What's a Cerebellar Circuit Doing in the Auditory System? *Trends Neurosci.* **2004**, *27*, 104−110.
(39) Frederickson, C. J.; Howell, G. A.; Haigh, M. D.; Danscher, G. Zinc-Containing Fiber Systems in the Cochlear Nuclei of the Rat and Mouse. *Hear. Res.* **1988**, *36*, 203−211.
(40) Perez-Rosello, T.; Anderson, C. T.; Schopfer, F. J.; Zhao, Y.; Gilad, D.; Salvatore, S. R.; Freeman, B. A.; Hershfinkel, M.; Aizenman, E.; Tzounopoulos, T. Synaptic Zn^{2+} Inhibits Neurotransmitter Release by Promoting Endocannabinoid Synthesis. *J. Neurosci.* **2013**, *33*, 9259−9272.
(41) Casey, J. R.; Grinstein, S.; Orlowski, J. Sensors and Regulators of Intracellular pH. *Nat. Rev. Mol. Cell Biol.* **2010**, *11*, 50−61.

DOI: 10.1021/acssensors.5b00022
ACS Sens. 2016, 1, 32−39